Catal Lett (2008) 126:155–163
DOI 10.1007/s10562-008-9598-y

Preparation of Mesoporous V–Ce–Ti–O for the Selective Oxidation of Methanol to Dimethoxymethane

Jingwei Liu · Qing Sun · Yuchuan Fu · Hongying Zhao · Aline Auroux · Jianyi Shen

Received: 30 April 2008 / Accepted: 22 July 2008 / Published online: 5 September 2008

Abstract Mesoporous V–Ce–Ti–O oxides were synthesized through the combination of sol–gel and hydrothermal methods and were characterized by different techniques. N_2 adsorption showed that the mesoporous oxides with 0–20 wt.% V_2O_5 possessed the surface areas of about 160 $m^2\ g^{-1}$ with narrow pore size distribution centered around 4–5 nm. Vanadium species were highly dispersed in the samples, as confirmed by the wide angle XRD and Raman spectroscopy. The surface acidity of the materials was determined by the microcalorimetric adsorption of NH_3. Temperature programmed reduction and O_2 chemisorption were used to probe the redox property of the materials. It was found that the mesoporous V–Ce–Ti–O possessed bifunctional characters of acidic and redox properties that catalyzed the oxidation of methanol to dimethoxymethane (DMM). These bifunctional characters were further enhanced by the addition of V_2O_5 and SO_4^{2-} onto V–Ce–Ti–O simultaneously. Such supported catalysts exhibited excellent performance for the selective oxidation of methanol to DMM. Specifically, 72% conversion of methanol with 85% selectivity to DMM was achieved at 423 K over a SO_4^{2-}–V_2O_5/V–Ce–Ti–O catalyst.

J. Liu · Q. Sun · Y. Fu · H. Zhao · J. Shen (✉)
Lab of Mesoscopic Chemistry, School of Chemistry and Chemical Engineering, Nanjing University, Nanjing 210093, China
e-mail: jyshen@nju.edu.cn

H. Zhao · A. Auroux
Institut de Recherches sur la Catalyse et l'Environnement de Lyon, UMR 5256, CNRS-Université Lyon 1, 2 Avenue Albert Einstein, 69626 Villeurbanne Cedex, France

Keywords Mesoporous V–Ce–Ti–O · Surface acidity · Surface redox property · Oxidation of methanol · Synthesis of dimethoxymethane

1 Introduction

V_2O_5/TiO_2 catalysts are extensively studied in various reactions such as selective oxidation of methanol to formaldehyde [1] and methyl formate [2], selective oxidation of aromatic compounds to aromatic aldehydes [3], selective oxidation of olefins to phthalic anhydride [4], ammoxidation of aromatic hydrocarbons [5] and selective catalytic reduction of NO_X [6]. It is generally true that the V_2O_5/TiO_2 with higher surface areas may work better since more vanadia species could be dispersed on the surface to act as active sites [7]. However, TiO_2 usually exhibits a moderate surface area of about 50 $m^2\ g^{-1}$ (e.g., Degussa P25) [1, 2]. Although mesoporous titanium oxides may provide a higher surface area to support more VO_x species, these materials were usually not thermally stable [8]. The surface areas of these materials might be greatly decreased upon the calcination at temperatures higher than 673 K. Doping with rare earth elements was proved to be an effective way to enhance the thermal stability of mesoporous materials [9, 10], in which cerium was recently reported as an excellent dopant in mesoporous titania [9]. In addition, cerium is known as an essential component for three-way catalysts (TWC) due to its oxygen storage capability. It also plays positive synergetic roles in some catalytic systems [11]. Therefore, Ce doped mesoporous titania might be used as supports for a variety of oxidation reactions.

Among the aforementioned reactions, the oxidation of methanol has been widely used as a probe reaction to

characterize the activity of oxide catalysts and to correlate the structures and surface acidic and redox properties [12]. It has been reported that methanol could be converted to dimethyl ether (DME) on acidic surface, to formaldehyde (FA) and methyl formate (MF) on oxidative surface, and to dimethoxymethane (DMM) on acidic and oxidative bifunctional surfaces [12].

In this work, mesoporous V–Ce–Ti–O materials were first synthesized through the combination of sol–gel and hydrothermal methods, and were characterized by X-ray diffraction (XRD), N_2 adsorption, transmission electron microscopy (TEM), O_2 chemisorption, laser Raman spectroscopy (LRS), temperature programmed reduction (TPR), and microcalorimetric adsorption of ammonia. The surface redox and acidic properties of the V–Ce–Ti–O could be enhanced by the addition of V_2O_5 and SO_4^{2-}. These materials were tested for the selective oxidation of methanol to DMM.

2 Experimental

2.1 Preparation of Samples

Mesoporous Ce–Ti–O has been synthesized by Yue and Gao [9]. In this work, mesoporous V–Ce–Ti–O materials were synthesized via the combination of sol–gel and conventional hydrothermal methods. In a typical procedure, 5.48 g P123 (triblock copolymer pluronic) and 0.89 g $CeCl_3 \cdot 7H_2O$ were dissolved in 25 mL absolute ethanol, and then 16.10 g titanium butoxide (TBOT) was added under vigorous stirring. Desired amounts of V_2O_5 were added into a mixed solution of 17.8 mL ethanol and 30% H_2O_2 under constant stirring, until V_2O_5 was completely dissolved. The molar ratio of V_2O_5/H_2O_2 was 0.22. Then, the solution containing vanadium was added dropwise into the solution containing titanium precursor at room temperature. The mixed solution formed was clear at first, and then became a gel in 10 min. A sample 20V–Ti–O without cerium cations was also prepared for comparison. A precipitate (no gel) was formed without the presence of cerium cations. The gel (or precipitate) together with 70 mL distilled water was subsequently transferred into a Teflon-lined autoclave and kept at 393 K for 24 h. Afterwards, the gel (or precipitate) was filtered, washed with deionized water and ethanol and dried at room temperature for 12 h. The samples were then calcined at 673 K for 5 h in air (temperature ramped at 1 K min^{-1}). The samples Ce–Ti–O, 10V–Ce–Ti–O, 20V–Ce–Ti–O, 40V–Ce–Ti–O and 20V–Ti–O prepared this way contained about 0, 10, 20, 40 and 20% V_2O_5 (wt.%), respectively.

The V_2O_5/V–Ce–Ti–O, SO_4^{2-}/V–Ce–Ti–O and SO_4^{2-}–V_2O_5/V–Ce–Ti–O samples were prepared by using the incipient wetness impregnation method. Specifically, for each preparation, a known amount of above mentioned V–Ce–Ti–O oxide was added into the aqueous solution containing the desired amount of vanadium oxalate and/or $Ti(SO_4)_2$ and stirred. After being kept at room temperature overnight, the impregnated samples were dried at 373 K and then calcined in air at 673 K for 5 h.

2.2 Characterization

Low angle and wide angle powder X-ray diffraction patterns were collected on the Philips X'Pert Pro diffractometer using Ni-filtered Cu Kα radiation ($\lambda = 0.15418$ nm), operated at 40 kV and 40 mA. Nitrogen adsorption–desorption isotherms were measured at liquid nitrogen temperature using a Micromeritics ASAP 2020. Prior to a measurement, the sample was degassed to 10^{-3} Torr at 573 K for 4 h. Pore size distribution and pore volume were calculated by the BJH method according to the desorption isotherm branch. Elemental analysis was performed on an ARL-9800 X-ray fluorescence spectrometer. TEM images were obtained from a JEOL JEM 2100 transmission electronic microscope with an accelerating voltage of 200 kV. The samples were dispersed in ethanol under ultrasonic conditions and deposited onto copper grids coated with ultrathin carbon films. Laser Raman spectra were acquired on a Renishaw inVia Raman microscope with the 514.5 nm line of an Ar ion laser as the excitation source of about 2 mW. Spectra were recorded with 1 cm^{-1} resolution and 20 scans.

The dispersion of vanadium species was measured by using the high temperature oxygen chemisorption method (HTOC). About 0.1–0.2 g sample was reduced in flowing H_2 (40 mL min^{-1}) at 640 K for 2 h, and evacuated at the same temperature for 0.5 h. Oxygen uptake was measured at 640 K.

Microcalorimetric adsorption of ammonia was performed at 423 K by using a Tian-Calvet type heat flux Setaram C80 calorimeter. The calorimeter was connected to a volumetric system equipped with a Baratron capacitance manometer for the pressure measurement and gas handling. About 0.1 g sample was pretreated in 500 Torr O_2 at 573 K for 1 h, followed by evacuation at the same temperature for 1 h. The probe molecule ammonia was purified with the successive freeze-pump-thaw cycles.

TPR measurements were carried out in a continuous mode using a U-type quartz micro-reactor (3.5 mm inner diameter). A sample of about 50 mg was contacted with a H_2:N_2 mixture (5.13% volume of H_2 in N_2) at a total flow rate of 40 mL min^{-1}. The sample was heated at a rate of 10 K min^{-1} from room temperature to 1250 K. The hydrogen consumption was monitored using a thermal conductivity detector (TCD).

2.3 Catalytic Reactions

The reaction of selective oxidation of methanol was carried out at atmospheric pressure in a fixed-bed micro-reactor (glass) with an inner diameter of 6 mm. Methanol was introduced into the reaction zone by bubbling O_2/N_2 (1/5) through a glass saturator filled with methanol (99.9%) maintained at 278 K. In each test, 0.2 g of catalyst was loaded, and the gas hourly space velocity (GHSV) was 11400 mL g^{-1} h^{-1}. The feed composition was maintained as methanol: O_2:N_2 = 1:3:15 (v/v). Methanol, DMM, formaldehyde and other organic compounds were analyzed by using a GC equipped with FID and TCD detectors connected to Porapak N columns. CO and CO_2 were detected by using another GC with a TCD connected to a TDX-01 column. The gas lines were kept at 373 K to prevent condensation of reactants and products.

3 Results and Discussion

3.1 Structure Characterization

Figure 1 presents the low angle XRD patterns of V–Ce–Ti–O samples. Only a single broad peak was observed for the samples with the content of V_2O_5 lower than 20%, indicating the mesostructure that lacked of long range order [13–15]. The intensity of this peak decreased gradually with the increase of V_2O_5 content, suggesting the increased disordered structures of the samples.

Figure 2 shows the wide angle XRD patterns for the V–Ce–Ti–O oxides. The diffraction peaks due to anatase were observed for all the samples. No other diffraction peaks were observed for the V–Ce–Ti–O samples with 0–20% of V_2O_5,

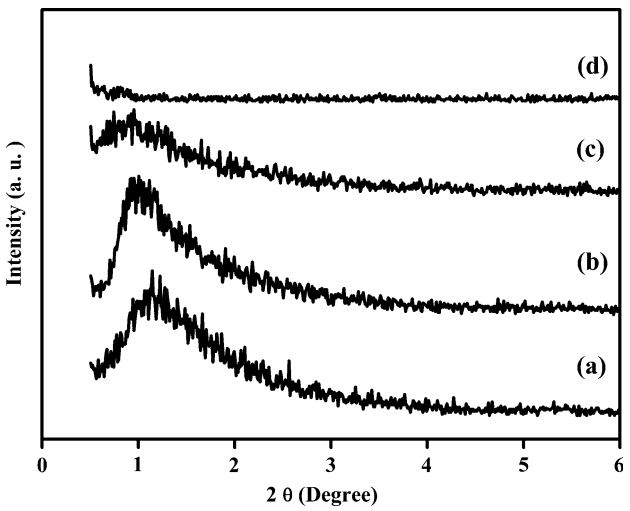

Fig. 1 Low angle XRD patterns of (**a**) Ce–Ti–O, (**b**) 10V–Ce–Ti–O, (**c**) 20V–Ce–Ti–O and (**d**) 40V–Ce–Ti–O

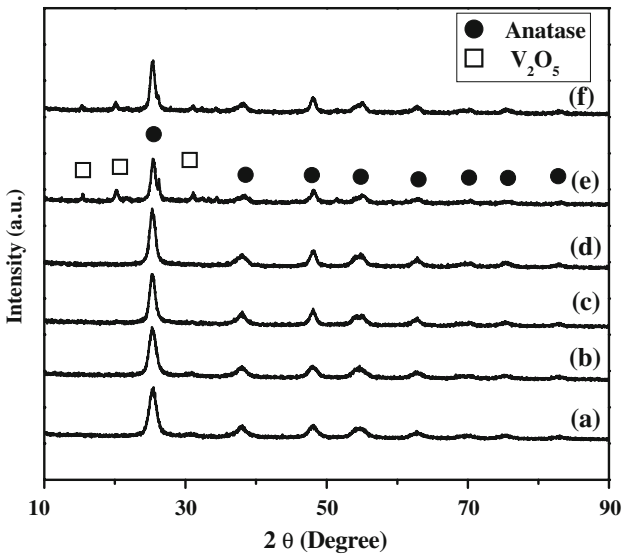

Fig. 2 Wide angle XRD patterns of (**a**) Ce–Ti–O, (**b**) 10V–Ce–Ti–O, (**c**) 10V/10V–Ce–Ti–O, (**d**) 20V–Ce–Ti–O, (**e**) 20V–Ti–O and (**f**) 40V–Ce–Ti–O

indicating that vanadia and ceria species were highly dispersed in the oxides. In the sample with 40% V_2O_5, weak diffraction peaks of crystalline V_2O_5 appeared, suggesting the occurrence of agglomeration of vanadia species. Crystalline V_2O_5 was also observed for the 20V–Ti–O without the presence of cerium. The 10V–Ce–Ti–O was used to support additional 10% V_2O_5, and the resulted 10V/10V–Ce–Ti–O displayed only the diffraction peaks of anatase, indicating the highly dispersed V_2O_5 on the surface of 10V–Ce–Ti–O. Figure 3 shows the nitrogen adsorption–desorption isotherms and corresponding BJH pore size distributions for the V–Ce–Ti–O oxides. The surface areas and pore parameters are summarized in Table 1. All the oxides prepared exhibited typical IV nitrogen isotherms, characteristic of mesoporous materials, according to the IUPAC classification [16]. Narrow pore size distributions were derived from the hysteresis loops as seen in the inserts of Fig. 3. The surface area, average pore size and pore volume for the Ce–Ti–O were found to be 160 m^2 g^{-1}, 5.2 nm and 0.3 cm^3 g^{-1}, respectively. With the incorporation of less than 20% V_2O_5, the surface areas of the formed V–Ce–Ti–O oxides changed little, while pore sizes and pore volumes decreased apparently. Further increase of V_2O_5 to 40% led to the significantly decreased surface area (62 m^2 g^{-1}) and increased pore size (12.7 nm). The surface area of the 20V–Ti–O (91 m^2 g^{-1}) was much lower than that of the corresponding 20V–Ce–Ti–O (159 m^2 g^{-1}), suggesting that cerium might play an important role in maintaining the thermal stability of the V–Ce–Ti–O oxides. Such effect of cerium was also reported by Radwan et al. [17]. Addition of 10% V_2O_5 on the 10V–Ce–Ti–O decreased the surface areas to about 130 m^2 g^{-1} and increased the pore sizes to about 7 nm. Simultaneous addition of V_2O_5 and SO_4^{2-} resulted in a

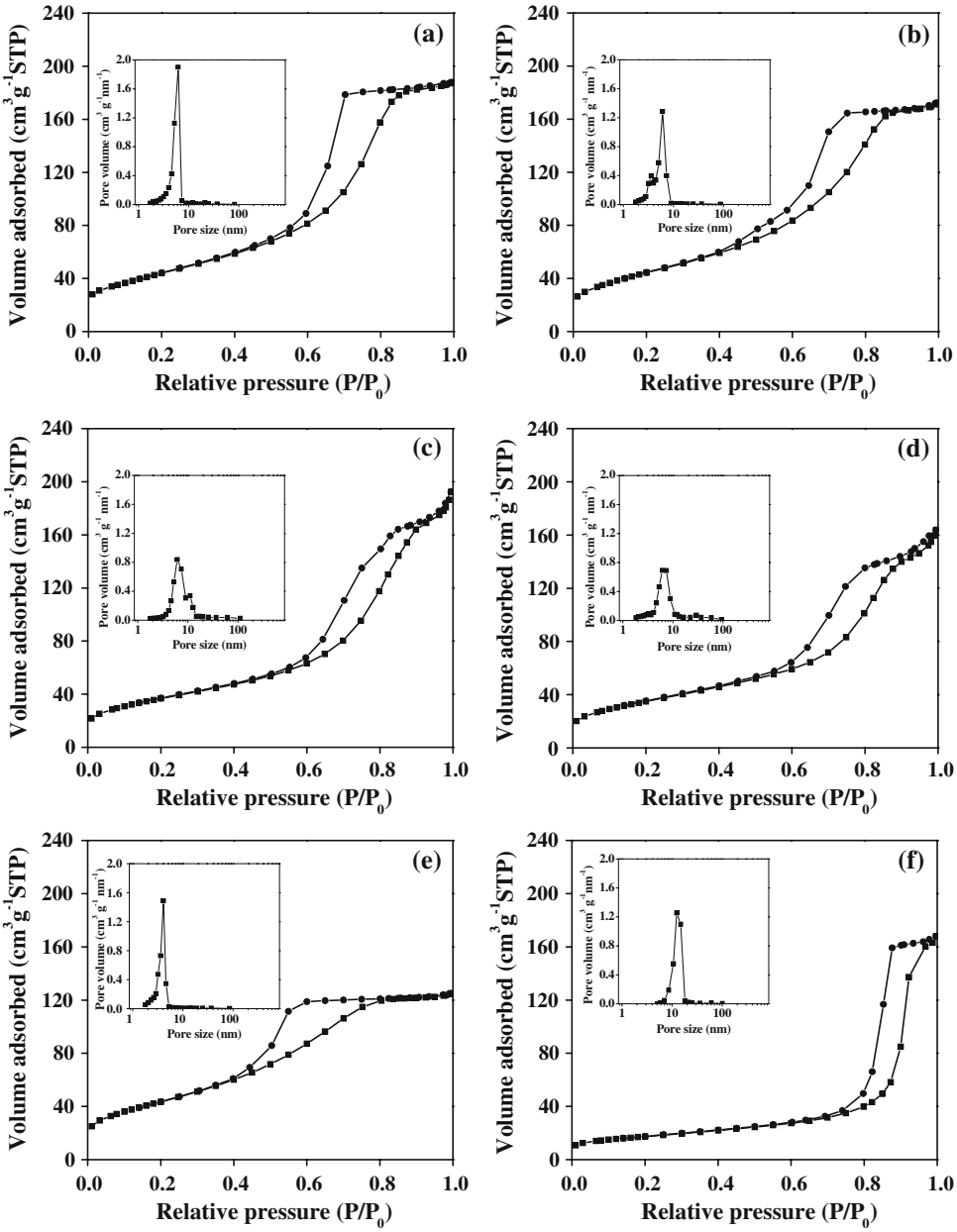

Fig. 3 Nitrogen adsorption–desorption isotherms and pore size distributions for (**a**) Ce–Ti–O, (**b**) 10V–Ce–Ti–O, (**c**) 10V/10V–Ce–Ti–O, (**d**) $5SO_4^{2-}$–10V/10V–Ce–Ti–O, (**e**) 20V–Ce–Ti–O and (**f**) 40V–Ce–Ti–O

Table 1 Surface areas, pore parameters and O_2 uptakes for the V–Ce–Ti–O samples

Sample	S_{BET} (m^2 g^{-1})	Pore size (nm)	Pore volume (cm^3 g^{-1})	O_2 uptake (μmol g^{-1})	V density calculated (V nm^{-2})
Ce–Ti–O	160	5.2	0.30	6	–
10V–Ce–Ti–O	162	5.0	0.27	534	4.0
20V–Ce–Ti–O	159	3.6	0.20	990	7.4
20V–Ti–O	91	8.4	0.31	861	11.3
40V–Ce–Ti–O	62	12.7	0.26	1516	29.4
10V/10V–Ce–Ti–O	134	7.2	0.30	870	7.8
$5SO_4^{2-}$–10V/10V–Ce–Ti–O	128	7.4	0.26	894	8.4

sample $5SO_4^{2-}$–10V/10V–Ce–Ti–O with the similar surface area and pore size as the 10V/10V–Ce–Ti–O.

The TEM images of 10V–Ce–Ti–O, 10V/10V–Ce–Ti–O and $5SO_4^{2-}$–10V/10V–Ce–Ti–O are shown in Fig. 4. No long range ordered structures were observed for the samples. Small particles (around 7 nm) with uniform size distribution were clearly seen for the 10V–Ce–Ti–O. Addition of 10% V_2O_5 only and simultaneous addition of 10% V_2O_5 and 5% SO_4^{2-} increased the particle size to about 10 nm. The mesoporosity of the V–Ce–Ti–O oxides was mainly due to the inter-particle voids.

The Raman spectra of the V–Ce–Ti–O oxides are presented in Fig. 5. It is well known that the bands around 149, 199, 408, 528 and 645 cm^{-1} are characteristic of anatase, whereas the bands around 144, 148, 611 cm^{-1} are ascribed to rutile phase [18]. Thus, all the V–Ce–Ti–O oxides studied in this work exhibited typical Raman features of anatase. No rutile phase was observed. Bulk CeO_2 usually exhibits a strong band at 460 cm^{-1} due to the F_{2g} Raman active mode characteristic of fluorite-structured materials [19]. The absence of the Raman line due to CeO_2 for all the V–Ce–Ti–O samples indicated the highly dispersed Ce^{4+} cations in the lattice of the samples, similar to the system of Ce–Ti–Cu–O oxides [20]. Additional Raman features around 800–1200 cm^{-1} observed are due to the different surface vanadia species. Only the Raman signals due to highly dispersed vanadia species were observed for the samples with V_2O_5 less than 40%. Specifically, the bands around 1024–1030 cm^{-1} could be assigned to isolated monomeric (or oligomeric) terminal V=O species [21], while the bands around 940 cm^{-1} and 830 cm^{-1} are characteristic of polymeric V–O–V species [22] and octahedral decavanadate species $V_{10}O_{28}$ [5, 23] (or isolated VO_4^{3-} tetrahedral structure [24]), respectively. When V_2O_5 reached 40%, a clear band at 999 cm^{-1} corresponding to V=O symmetric stretching vibration of crystalline V_2O_5 was discerned, indicating the formation of crystalline V_2O_5. Addition of 10% V_2O_5 onto the 10V–Ce–Ti–O did not result in new Raman features as compared with those of 10V–Ce–Ti–O, suggesting again that the additional V_2O_5 was highly dispersed on the 10V–Ce–Ti–O, in accordance with XRD results. In addition, the modification of SO_4^{2-} on the 10V/10V–Ce–Ti–O did not influence the dispersion of vanadia species (spectrum not shown).

3.2 Surface Redox and Acidic Properties

The adsorption of O_2 has been used to evaluate the dispersion of supported V_2O_5 [25–27]. Parekh and Weller [25, 26] proposed a low temperature oxygen adsorption method (LTOC) while Oyama et al. suggested a high temperature oxygen adsorption method (HTOC) [27].

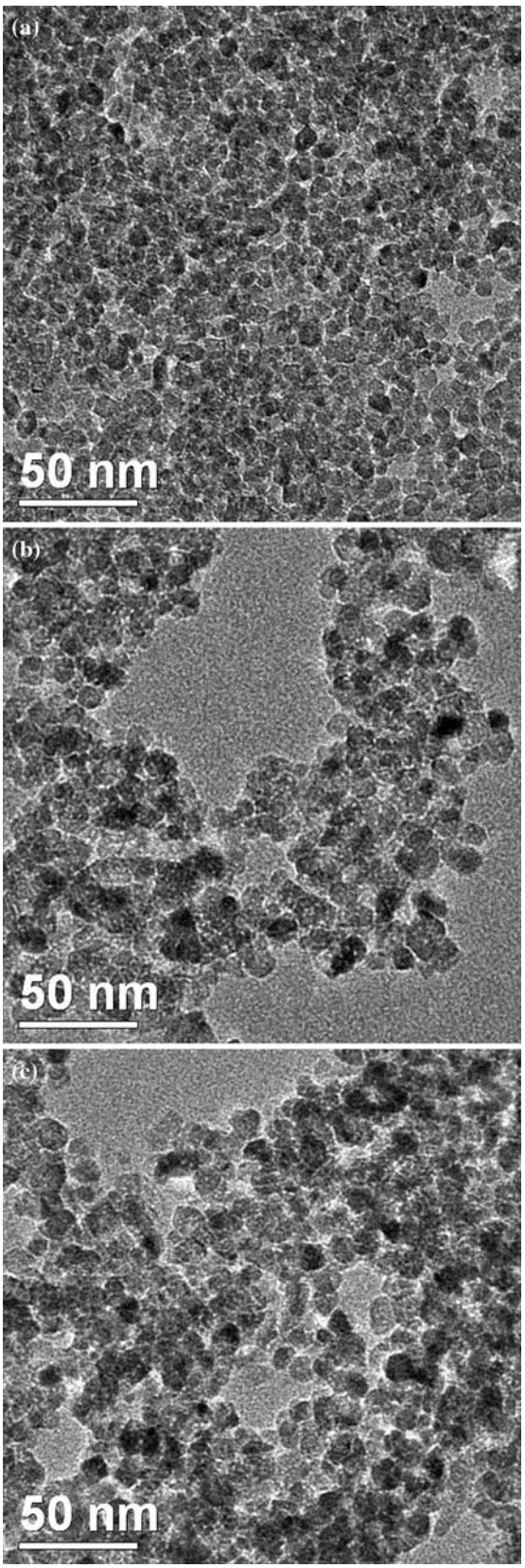

Fig. 4 Transmission electron microscopy (TEM) images of (**a**) 10V–Ce–Ti–O, (**b**) 10V/10V–Ce–Ti–O and (**c**) $5SO_4^{2-}$–10V/10V–Ce–Ti–O

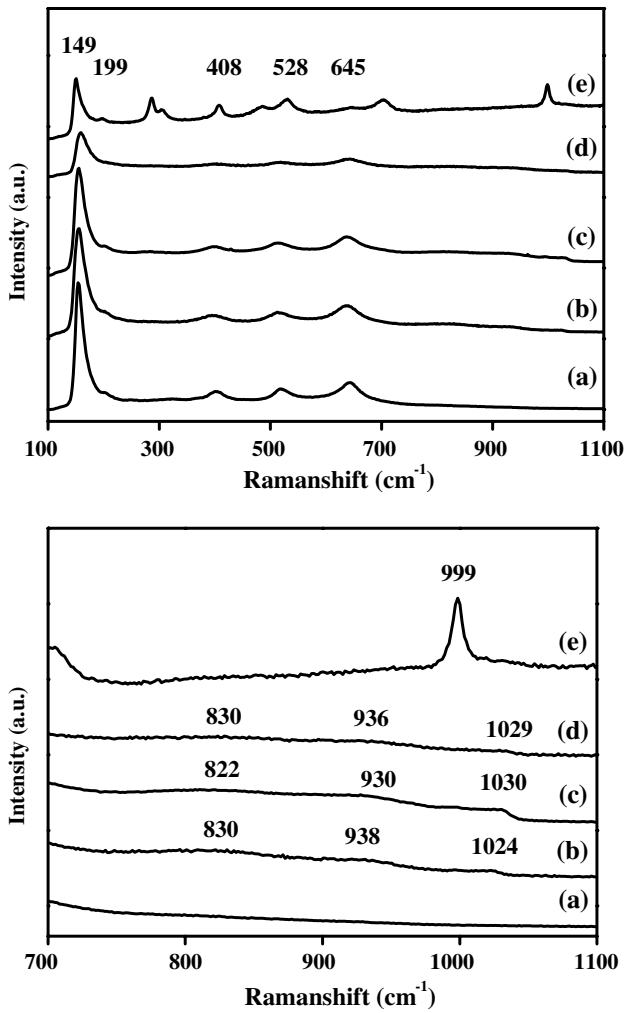

Fig. 5 Raman spectra of (**a**) Ce–Ti–O, (**b**) 10V–Ce–Ti–O, (**c**) 10V/10V–Ce–Ti–O, (**d**) 20V–Ce–Ti–O and (**e**) 40V–Ce–Ti–O

It was suggested that the HTOC might exert less possibility of bulk reduction and sintering [28], and we used the technique to estimate roughly the dispersion of vanadium species. In this technique, the samples were first reduced in H_2 at 640 K, at which only surface vanadium species were supposedly reduced [27]. O_2 adsorption was then performed at 640 K to titrate the number of reduced vanadium cations on the surface with the ratio of O/V = 1.

Table 1 gives the O_2 uptakes and corresponding V densities for the different V–Ce–Ti–O oxides. It is seen that the Ce–Ti–O did not seem to adsorb O_2 (6 μmol g^{-1} only), indicating that little species could be reduced in the sample (or non-redox). The incorporation of vanadium species increased the O_2 uptakes. Since the Ce–Ti–O almost did not adsorb O_2, O_2 was mainly adsorbed on vanadium species in the V–Ce–Ti–O samples. Wachs [29] reported that the theoretical density for the monolayerly dispersed vanadium species on TiO_2 was 7.9 V nm^{-2}. Since the 10V–Ce–Ti–O possessed 9.6% V_2O_5 (measured by XRF, see Table 2) and the surface area of 162 m^2 g^{-1}, the density of vanadium species was calculated to be 3.9 V nm^{-2}, lower than the monolayer capacity. The surface density of vanadium as titrated by O_2 adsorption for the sample was 4.0 V nm^{-2}, almost same as the amount of vanadium contained in the sample. This implied that all the vanadium species in the 10V–Ce–Ti–O sample were titrated by the O_2 adsorption at 640 K. Similarly, the 20V–Ce–Ti–O and 10V/10V–Ce–Ti–O contained vanadium species of 7.5 and 9.0 V nm^{-2}, according to their surface areas in Table 1 and the contents of V_2O_5 in Table 2. The titrated surface densities of vanadium in the two samples were 7.4 and 7.8 V nm^{-2}, respectively, suggesting again that the O_2 adsorption at 640 K titrated most of the vanadium species in the samples. The content of V_2O_5 in the 40V–Ce–Ti–O was not measured. Supposing it contained 40% V_2O_5 with the surface area of 62 m^2 g^{-1}, the density of vanadium was calculated to be 42.7 V nm^{-2}. The surface density of vanadium for this sample as titrated by O_2 adsorption was 29.8 V nm^{-2}, much greater than the monolayer dispersion capacity (7.9 V nm^{-2}), indicating that the HTOC technique did titrate sublayers of vanadia species. Without the presence of Ce, the 20V–Ti–O exhibited lower surface

Table 2 Selective oxidation of methanol over different catalysts at 423 K

Catalyst	Content[a] (wt.%)			Conv. (%)	Selectivity (%)			
	Ce	V_2O_5	SO_4^{2-}		DMM[b]	FA[b]	MF[b]	DME[b]
Ce–Ti–O	1.6	–	–	0.9	0	0	0	100
10V–Ce–Ti–O	1.5	9.6	–	12	62	22	16	0
20V–Ce–Ti–O	1.1	18.0	–	31	26	22	51	1
20V–Ti–O	–	–	–	22	48	40	11	1
2.5SO_4^{2-}/20V–Ce–Ti–O	1.0	17.8	2.5	40	91	1	7	1
10V/10V–Ce–Ti–O	1.3	18.2	–	29	52	18	29	1
5SO_4^{2-}–10V/10V–Ce–Ti–O	1.3	17.7	5.5	72	85	0	14	1

[a] The contents of Ce, V_2O_5 and SO_4^{2-} were measured by XRF

[b] DMM = dimethoxymethane; FA = formaldehyde; DME = dimethyl ether; MF = methyl formate

area as compared to the 20V–Ce–Ti–O, leading to the lower O_2 uptake and lower dispersion of vanadium species.

Temperature programmed reduction (TPR) is a technique usually used to characterize the reducibility of various metal oxides or supported catalysts. Figure 6 shows the TPR profiles of different V–Ce–Ti–O samples. No TPR peaks were observed for the Ce–Ti–O, indicating the non-redox feature of the sample, consistent with the result of O_2 adsorption. Two TPR peaks can be seen for the 10V–Ce–Ti–O around 775 and 797 K, which might be ascribed to the reduction of monomeric and polymeric surface VO_x species from V^{5+} to V^{3+} [30, 31]. These two peaks shifted to higher temperatures with the increase of vanadia content. Addition of 10% V_2O_5 on the 10V–Ce–Ti–O did not seem to change the TPR profile, but increased the peak intensities. Bulk V_2O_5 displayed a completely different reduction feature, which has been discussed thoroughly before [32]. The significantly lower reduction temperatures for the V–Ce–Ti–O than for bulk V_2O_5 suggested the enhanced reducibility (or redox ability) of the V–Ce–Ti–O samples.

Microcalorimetric adsorption of ammonia has been used to determine the number, strength and strength distribution of surface acidities [33]. Differential heats versus coverage for NH_3 adsorption on the V–Ce–Ti–O samples are depicted in Fig. 7. The Ce–Ti–O exhibited the initial adsorption heat of 151 kJ mol^{-1} with NH_3 saturation coverage of 2.6 μmol m^{-2}. The incorporation of V into the Ce–Ti–O enhanced the surface acidity since both the initial heat and saturation coverage of NH_3 increased. Specifically, the initial heat and ammonia coverage increased to 183 kJ mol^{-1} and 4 μmol m^{-2}, respectively, for the 10V–Ce–Ti–O. Addition of SO_4^{2-} into V–Ce–Ti–O also increased the surface acidity. For example, addition of 2.5% SO_4^{2-} into the 20V–Ce–Ti–O increased the initial heat from 158 to 173 kJ mol^{-1} and the saturation coverage of ammonia from 3.5 to 4.4 μmol m^{-2}. However, when more SO_4^{2-} (5.5%) was added into the 10V/10V–Ce–Ti–O, much lower initial heat (15 kJ mol^{-1}) was measured, due to the endothermic interaction of ammonia with polymerized surface sulfates. Similar phenomenon was also reported by Desmartin-Chomel et al. for the sulfated titania, and the existence of polymerized sulfate species were observed by FTIR [34]. Thus, the initial heat of ammonia adsorption for the samples with high contents of SO_4^{2-} cannot be used as an indication of strength of surface acidity. However, it is clear that the density of acid sites as determined by the adsorption of ammonia was significantly higher for the 5% SO_4^{2-}–10V/10V–Ce–Ti–O (4.6 μmol m^{-2}) than for the 10V/10V–Ce–Ti–O (3.9 μmol m^{-2}). The sample SO_4^{2-}/20V–Ce–Ti–O with 2.5% SO_4^{2-} did not show the decreased initial heat. This might be an indication that no polymerized surface sulfates were formed in the 2.5SO_4^{2-}/20V–Ce–Ti–O [34].

Infrared spectroscopy for ammonia adsorption is a frequently used tool to probe the surface acidity (Brønsted and Lewis sites). The FTIR spectra of adsorbed NH_3 for the V–Ce–Ti–O samples are presented in Fig. 8. The Ce–Ti–O

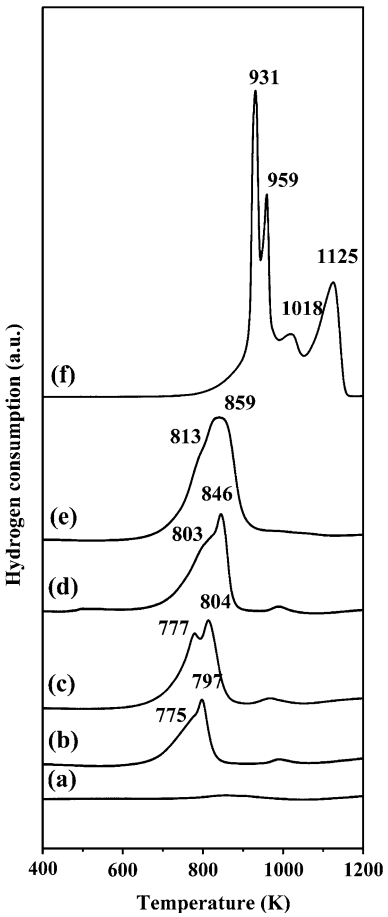

Fig. 6 TPR profiles of (**a**) Ce–Ti–O, (**b**) 10V–Ce–Ti–O, (**c**) 10V/10V–Ce–Ti–O, (**d**) 20V–Ce–Ti–O, (**e**) 40V–Ce–Ti–O and (**f**) V_2O_5

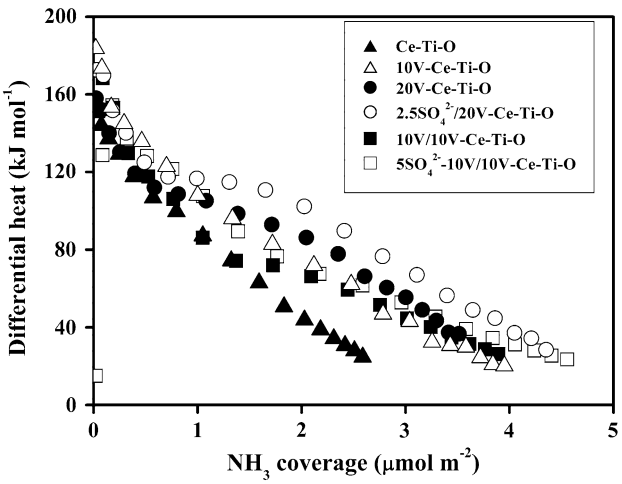

Fig. 7 Differential heat versus coverage for NH_3 adsorption at 423 K over the V–Ce–Ti–O catalysts

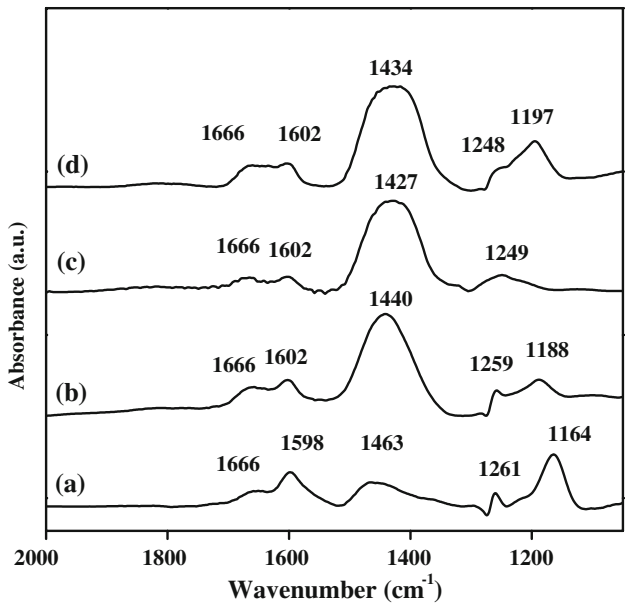

Fig. 8 FTIR spectra for NH_3 adsorption on (**a**) Ce–Ti–O, (**b**) 10V–Ce–Ti–O, (**c**) 10V/10V–Ce–Ti–O and (**d**) $5SO_4^{2-}$–10V/10V–Ce–Ti–O collected at room temperature

exhibited the bands at 1598, 1261 and 1164 cm^{-1}, belonging to NH_3 coordinately adsorbed on Lewis acid sites [34]. The bands at 1666 and 1463 cm^{-1} were related to the adsorbed NH_3 on Brønsted acid sites [34]. Figure 8 shows that the Ce–Ti–O possessed mainly Lewis acidity with only weak Brønsted acidity. The incorporation of 10% V_2O_5 into Ce–Ti–O greatly enhanced the Brønsted acidity, as illustrated by the increased intensity around 1440 cm^{-1}. The enhanced surface Brønsted acidity might be created by the hydroxyl groups on the vanadia species in the 10V–Ce–Ti–O. The Lewis acidity with the band around 1164–1188 cm^{-1} due to the surface of Ce–Ti–O was still seen in the 10V–Ce–Ti–O. This band disappeared when additional 10% V_2O_5 was added into the 10V–Ce–Ti–O, probably due to the covering of Ce–Ti–O surface by dispersed V_2O_5. The band around 1249 cm^{-1} could be ascribed to the Lewis sites on the surface of dispersed V_2O_5. Further addition of 5% SO_4^{2-} on the 10V–Ce–Ti–O did not seem to increase the surface Brønsted acidity. In stead, a band around 1197 cm^{-1} appeared, which was owing to the Lewis acidic sites generated upon the addition of sulfate. The generation of Lewis acid sites due to the addition of sulfate on TiO_2 has been reported elsewhere [34].

3.3 Selective Oxidation of Methanol to Dimethoxymethane

Methanol and its derivatives have been widely studied due to their industrial importance [12]. In addition, the catalytic oxidation of methanol is a convenient structure-sensitive reaction, which has been widely used to characterize the surfaces of metal oxides for their acid/base and redox properties [12, 35]. The results for the conversion of methanol over the Ce–Ti–O and V–Ce–Ti–O catalysts under oxidative atmosphere were given in Table 2.

The data in Table 2 showed that the conversion of methanol was very low (0.9%) over the Ce–Ti–O at 423 K. The only product was DME. This is due to that the Ce–Ti–O was lack of redox property, as evidenced by the results of O_2 adsorption and TPR. Incorporation of V into Ce–Ti–O drastically improved the activity of selective oxidation of methanol. For example, the conversion of methanol on the 10V–Ce–Ti–O was 12% with DMM as the main product (62%). The increased activity and selectivity to DMM were due to the enhanced surface acidic and redox properties of the V–Ce–Ti–O. The 20V–Ce–Ti–O sample exhibited higher methanol conversion and higher selectivity to MF than the 10V–Ce–Ti–O. The 20V–Ti–O exhibited lower methanol conversion than the 20V–Ce–Ti–O and produced more formaldehyde. Addition of 2.5% SO_4^{2-} into the 20V–Ce–Ti–O increased the conversion of methanol from 31 to 40% and the selectivity to DMM from 26 to 91%, owing to the enhanced surface acidity. It has been reported that the selective oxidation of methanol to DMM might involve two steps: (1) oxidation of methanol to formaldehyde on redox sites and (2) condensation of formaldehyde produced with additional methanol to DMM on acidic sites. Thus, the strengths of surface acidity and redox ability of a catalyst were two important aspects in determining the selective oxidation of methanol to DMM [36–40].

Addition of V_2O_5 and SO_4^{2-} onto V–Ce–Ti–O enhanced further the surface redox and acidic properties. For example, the addition of 10% V_2O_5 onto 10V–Ce–Ti–O increased the conversion of methanol from 12 to 29% and the selectivity to MF from 16 to 29%, due to the enhanced surface redox ability. Further addition of 5.5% SO_4^{2-} increased the conversion of methanol from 29 to 72% and the selectivity to DMM from 52 to 85%, owing to the enhanced surface acidity. The selectivity of DMM was quite high (85%) over the SO_4^{2-}–10V/10V–Ce–Ti–O, even at high conversion of methanol (72%). This result appears promising for the industrial application. Thus, we demonstrated in this work that the mesoporous V–Ce–Ti–O oxides could act as the appropriate supports for V_2O_5 and SO_4^{2-} to achieve the excellent performance for the selective oxidation of methanol to DMM.

4 Conclusion

Mesoporous V–Ce–Ti–O materials were successfully synthesized via a combination of sol–gel and hydrothermal methods, which possessed the surface areas of about 160 $m^2\ g^{-1}$ and pore sizes of about 4–5 nm. Such

materials exhibited weak surface acidity and redox ability that could be significantly enhanced by the addition of V_2O_5 and SO_4^{2-} simultaneously on the surface, leading to the bi-functional catalysts with strong acidic and redox characters that favored the selective oxidation of methanol to dimethoxymethane. Specifically, the 5% SO_4^{2-}–10% V/10% V–Ce–Ti–O exhibited the excellent performance for the selective oxidation of methanol to DMM. The conversion of methanol reached 72% over the 5% SO_4^{2-}–10% V/10% V–Ce–Ti–O with 85% selectivity to DMM at 423 K.

Acknowledgment We acknowledge the financial supports from NSFC (20673055) and MSTC (2004DFB02900 and 2005CB221400).

References

1. Roozeboom F, Cordingley PD, Gellings PJ (1981) J Catal 68:464
2. Elmi AS, Tronconi E, Cristiani C, Gomez Martin JP, Forzatti P, Busca G (1989) Ind Eng Chem Res 28:387
3. Maurya SK, Patil P, Umbarkar SB, Gurjar MK, Dongare M, Rudiger S, Kemnitz E (2005) J Mol Catal A 234:51
4. Cavani F, Cortelli C, Frattini A, Panzacchi B, Ravaglia V, Trifiro F, Fumagalli C, Leanza R, Mazzoni G (2006) Catal Today 118:298
5. Sanati M, Andersson A (1990) J Mol Catal 59:233
6. Mutin PH, Popa AF, Vioux A, Delahay G, Coq B (2006) Appl Catal B 69:49
7. Shyue JJ, De Guire MR (2005) J Am Chem Soc 127:12736
8. Yang P, Zhao D, Margolese DI, Chmelka BF, Stucky GD (1998) Nature 396:152
9. Yue Y, Gao Z (2000) Chem Commun 1755
10. Severin KG, Abdel-Fattah TM, Pinnavaia TJ (1998) Chem Commun 1471
11. Terribile D, Llorca J, Boaro M, de Leitenburg C, Dolcetti G, Trovarelli A (1998) Chem Commun 1897
12. Tatibouet JM (1997) Appl Catal A 148:213
13. Luo H, Wang C, Yan Y (2003) Chem Mater 15:3841
14. Kartini I, Menzies D, Blake D, da Costa JCD, Meredith P, Riches JD, Lu GQ (2004) J Mater Chem 14:2917
15. Khushalani D, Ozin GA, Kuperman A (1999) J Mater Chem 9:1491
16. Gregg SJ, Sing KS (1982) Adsorption, surface area and porosity. Academic Press, New York
17. Radwan NRE, Fagal GA, El-Shobaky GA (2001) Colloids Surf A 178:277
18. Kosmulski M (2002) Adv Colloid Interface Sci 99:255
19. Reddy BM, Khan A, Yamada Y, Kobayashi T, Loridant S, Volta JC (2003) J Phys Chem B 107:5162
20. Francisco MSP, Mastelaro VR, Nascente PAP, Florentino AO (2001) J Phys Chem B 105:10515
21. Machej T, Haber J, Turek AM, Wachs IE (1991) Appl Catal 70:115
22. Zhao C, Wachs IE (2006) Catal Today 118:332
23. Went GT, Oyama ST, Bell AT (1990) J Phys Chem 94:4240
24. Went GT, Leu LJ, Bell AT (1992) J Catal 134:479
25. Roozeboom F, Mittelmeijer-Hazeleger MC, Moulijn JA, Medema J, De Beer VHJ, Gellings PJ (1980) J Phys Chem 84:2783
26. Parekh BS, Weller SW (1977) J Catal 47:100
27. Oyama ST, Went GT, Lewis KB, Bell AT, Somorjai GA (1989) J Phys Chem 93:6786
28. Arena F, Frusteri F, Parmaliana A (1999) Appl Catal A 176:189
29. Wachs IE (1996) Catal Today 27:437
30. Besselmann S, Freitag C, Hinrichsen O, Muhler M (2001) Phys Chem Chem Phys 3:4633
31. Poelman H, Sels BF, Olea M, Eufinger K, Paul JS, Moens B, Sack I, Balcaen V, Bertinchamps F, Gaigneaux EM, Jacobs PA, Marin GB, Poelman D, De Gryse R (2007) J Catal 245:156
32. Bosch H, Kip BJ, Ommen JGv, Gellings PJ (1984) J Chem Soc Faraday Trans 180:2479
33. Auroux A (1997) Top Catal 4:71
34. Desmartin-Chomel A, Flores JL, Bourane A, Clacens JM, Figueras F, Delahay G, Fendler AG, Lehaut-Burnouf C (2006) J Phys Chem B 110:858
35. Badlani M, Wachs IE (2001) Catal Lett 75:137
36. Sun Q, Fu Y, Liu J, Auroux A, Shen J (2008) Appl Catal A 334:26
37. Fu Y, Shen J (2007) Chem Commun 2172
38. Liu H, Bayat N, Iglesia E (2003) Angew Chem Int Ed 42:5072
39. YuanY, Shido T, Iwasawa Y (2000) Chem Commun 1421
40. Royer S, Sécordel X, Brandhorst M, Dumeignil F, Cristol S, Dujardin C, Capron M, Payen E, Dubois J (2008) Chem Commun 865